

# Polarizing the electronic and nuclear spin of the NV-center in diamond in arbitrary magnetic fields: analysis of the optical pumping process

Tanmoy Chakraborty, Jingfu Zhang and Dieter Suter

*Fakultät Physik, Technische Universität Dortmund, D-44221 Dortmund, Germany*

Initializing a set of qubits to a given quantum state is a basic prerequisite for the physical implementation of quantum-information protocols. Here, we discuss the polarization of the electronic and nuclear spin in a single Nitrogen vacancy center in diamond. Our initialization scheme uses a sequence of laser, microwave and radio-frequency pulses, and we optimize the pumping parameters of the laser pulse. A rate equation model is formulated that explains the effect of the laser pulse on the spin system. We have experimentally determined the population of the relevant spin states as a function of the duration of the laser pulse by measuring Rabi oscillations and Ramsey-type free-induction decays. The experimental data have been analyzed to determine the pumping rates of the rate equation model.

## I. INTRODUCTION

The nitrogen-vacancy (NV) center in diamond [1] has been identified as an excellent solid state quantum bit system, which provides the possibility of implementing quantum protocols at room temperature [2–4]. Most of these applications use the long coherence times of the NV center [5] and the optical initialization and readout of the system [6–8]. The NV center has been used for several interesting demonstrations like robust multipartite entanglement persisting over a timescale of milliseconds at room temperature [4], quantum interference between photons [9, 10], an efficient quantum memory [11–13], single shot readout of single nuclear spins [14] or quantum gate operations where dephasing is protected with the help of dynamical decoupling [15]. These developments of quantum information processing based on the defect centers in diamond have remarkably boosted solid state quantum technology and pioneered a new way towards reliable implementation of quantum computation [16].

For diamond crystals with low density of spins [17], it is possible to find single NV centers which remain magnetically well isolated from other defect centers. An NV center, consisting of the electronic spin and one or several nuclear spins, is therefore an interesting physical realization of a quantum register. Local control of the targeted qubits within a single NV center can be performed by specifically addressing the concerned center and manipulating the system with laser pulses, microwave (MW) and radio-frequency (RF) magnetic fields [18]. [19, 20]. Nuclear spins are useful resources for storing and transmitting quantum information [21, 22]. It is necessary to enhance the strength of nuclear spin polarization since it improves the efficiency of detection of nuclear magnetic resonance (NMR) signal and hence increases the signal-to-noise ratio. In this context, DNP (dynamic nuclear polarization)[23, 24] has been widely established as an effective technique which relies on transferring the spin polarization from electrons to nuclei. Optically induced DNP [25, 26] has been successfully applied to polarize the nuclear spins in systems like diamond [27–29] and

silicon carbide [30]. Other novel approaches include high fidelity nuclear spin initialization and single shot read out at excited state level anticrossing[31–33], implementation of Hartmann-Hahn double resonance technique[28, 34], population trapping protocols [13, 19, 20] etc. However, the resulting polarization using certain pulse sequences [13, 19, 20], like a scheme presented through this paper, are limited by the fact that the initialization technique in the beginning using a long laser pulse although can create a strong electronic polarization, it cannot completely initialize the system into the  $m_S = 0$  state [35]. On the other hand, such techniques have the advantage that these experiments do not require any specific magnetic field value.

In the present work, we discuss the initialization of a quantum register, which is an essential prerequisite for the implementation of a universal quantum computer [36]. In particular, we investigate a protocol for polarizing the electronic and the  $^{14}\text{N}$  nuclear spin of a single NV center in diamond. We have employed a sequence of pulses which is quite similar to what has been described in Ref. [20], where Pagliero et al. have employed MW, RF and laser pulses to polarize the nuclear spins associated with NV centers. However, the primary focus of our paper is optimizing the pulse sequence, evaluating the optical control parameters for the spins which play a substantial role in this initialization scheme and determining the purity of the relevant individual states by performing partial state tomography. For this purpose, we introduce a rate equation model which can explain the influence of optical irradiation on the spins and provide a physical picture of population transfer between different quantum states of the system. Thus, determination of the laser pumping parameters by analyzing the experimental data will help in initializing a quantum register to a target state in a more deterministic and optimized way. While the initialization of the electronic spin is a standard element of all applications of the NV center, it is more difficult to control the nuclear spin. To tackle this issue, the excited state level anti-crossing in a magnetic field has been used [37, 38]. The present technique does not rely on the anti-crossing and can therefore be applied at all strengths and

orientations of the magnetic field. The sequence starts with the usual initialization of the electronic spin by a laser pulse. We then swap the electronic and the nuclear spin and apply a second laser pulse to re-initialize the electron spin. Since the optical initialization procedure partly depolarizes the nuclear spin, it is important to understand the dynamics of the coupled spin system and to optimize the sequence such that the purity of the targeted state is maximized.

In the following, we discuss the system of interest and describe the initialization scheme. We then analyze the dynamics of the system in the presence of non-resonant optical irradiation and use the results for an optimal state preparation.

## II. SYSTEM AND SETUP

A single NV center embedded in a  $^{12}\text{C}$ -enriched (concentration of 99.995%) diamond sample was chosen as the experimental system. The effective dephasing time  $T_2^*$  for this center is  $\sim 40\mu\text{s}$ , as measured by a Ramsey-type free-induction decay experiment. The Hamiltonian of the system consisting of an electronic spin ( $S=1$ ) coupled to a  $^{14}\text{N}$  nuclear spin ( $I=1$ ) is

$$\mathcal{H} = DS_z^2 - \gamma_e BS_z + PI_z^2 - \gamma_n BI_z + AS_z I_z, \quad (1)$$

where  $D=2.87$  GHz is the zero-field splitting,  $S_z$  and  $I_z$  are the  $z$ -components of the electronic and nuclear spin operators,  $A = -2.16$  MHz is the hyperfine coupling,  $\gamma_n = 3.1$  MHz/T and  $\gamma_e = -28$  GHz/T are the nuclear and electronic gyromagnetic ratios and  $P = -4.95$  MHz represents the nuclear quadrupole coupling. Here, we assume that the magnetic field is oriented along the NV symmetry axis.

The measurements were performed at room temperature on a single NV center embedded in a diamond crystal. A diode-pumped solid-state laser emitting green light at 532 nm was employed for exciting the NV center in a home-built confocal microscope. The CW laser beam was passed through an acousto-optic modulator (AOM) with a rise time of 50 ns and an extinction ratio of 58 dB to generate pulses. The beam was then focused on a single NV center with a microscope objective (numerical aperture = 1.4) mounted on a nano-positioning system. The optical power at the sample was  $\sim 150\mu\text{W}$ . A MW signal generator (APSIN) and a direct digital synthesis (DDS) radio-frequency (RF)-source were used to generate the microwave (MW) signal, which was subsequently passed through a switch and an amplifier to create the MW pulses with suitable frequency, amplitude and phase for manipulating the electronic spins. Another DDS, switch and amplifier were used to generate the RF pulses for manipulating the nuclear spins. The MW and the RF pulses were passed through a combiner and a Cu wire attached to the surface of the sample. A permanent

magnet generated a magnetic field of 6.1 mT along the axis of the NV center.

## III. INITIALIZATION PROCEDURE AND THE RATE-EQUATION MODEL

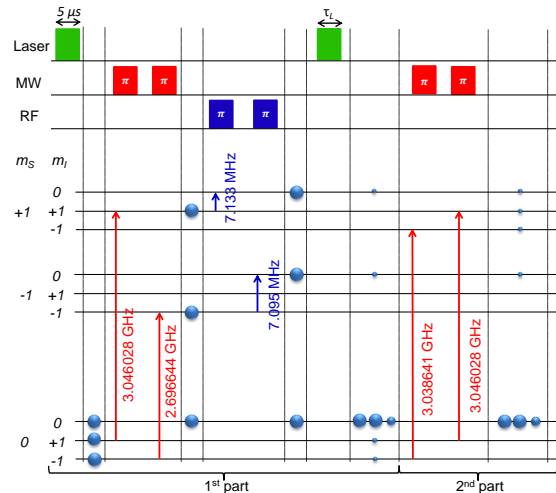


FIG. 1: Pulse sequence for initializing the system into the  $|0,0\rangle$  state. The occupation probability of the energy states have been schematically represented by the size of the filled circles. MW = microwave, RF = radio frequency. The time interval between the laser, MW and RF pulses were  $\approx 2\mu\text{s}$  which hardly affects the initialization scheme as the  $T_1$  for both the electronic and nuclear spin are  $\sim \text{ms}$ .

Fig. 1 shows the eigenstates and the transition frequencies between the relevant energy levels. To illustrate the pulse sequence in a convenient way, we list the states  $|m_S, m_I\rangle$  in the following order  $(m_S, m_I) = (0,-1; 0,+1; 0,0; -1,-1; -1,+1; -1, 0; +1,-1; +1,+1; +1,0)$  from the bottom to the top in the energy level scheme of Fig. 1 (the actual sequence of energies is slightly different), and in subsequent parts of the article.

The initialization process, which is also represented in Fig. 1 starts with a long ( $5\mu\text{s}$ ) laser pulse, which initializes the electronic spin into the bright ( $m_S = 0$ ) state, while the nuclear spin is fully depolarized. As mentioned earlier, it cannot completely initialize the system into the  $m_S = 0$  state and the actual polarization is usually unknown where different values are found in the literature. However, for the purpose of this paper, it is sufficient to determine the populations relative to the initial population of the  $m_S = 0$  state. Accordingly, conservation of populations implies that the sum of all populations must always be unity,  $\sum_{i=1}^9 P_i = 1$ . Also, we consider only the electronic ground state of the  $\text{NV}^-$  system, since the excited state population as well as the population of the  $\text{NV}^0$  states are small under our experimental conditions (excitation with 532 nm laser light) [39, 40]. After the

5  $\mu\text{s}$  laser pulse, two MW  $\pi$  pulses swap the populations of the  $|0, +1\rangle \leftrightarrow |+1, +1\rangle$  and the  $|0, -1\rangle \leftrightarrow |-1, -1\rangle$  states. Their pulse durations were 3.874  $\mu\text{s}$  and 1.456  $\mu\text{s}$ , respectively. Two RF pulses swap the populations between the nuclear spin states  $|+1, +1\rangle \leftrightarrow |+1, 0\rangle$  and  $|-1, -1\rangle \leftrightarrow |-1, 0\rangle$ ; both pulses had the same duration of 105.908  $\mu\text{s}$ . This sequence of four pulses thus exchanges the polarizations of the electronic and the nuclear spin: the nuclear spin becomes fully polarized in the  $m_I = 0$  state, but the electron spin becomes fully depolarized. The electronic spin therefore has to be re-polarized by a second laser pulse. Since this laser pulse affects not only the electronic spin, but also the nuclear spin, we have to analyze its effect on the spin system and optimize its duration. The 2<sup>nd</sup> part of Fig. 1 shows an additional purification step that can be used to remove population from the ground state that is not in the  $m_I = 0$  nuclear spin state.

We consider the effect of the laser on the spin system as a simple redistribution of populations between the different eigenstates of the spin Hamiltonian. We write  $\vec{P}$  for the populations of the nine states and use the sequence of states defined in Fig. 1. Writing  $k_S$  for the rate with which the electron spin changes from the  $m_S = \pm 1$  state to the  $m_S = 0$  state and  $k_I$  for the rate at which the nuclear spin flips between any pair of states, the equation of motion can be expressed in matrix form as

$$\frac{d}{dt} \vec{P} = M(k_S, k_I) \vec{P}, \quad (2)$$

with the full form of the matrix  $M$  given in the appendix. Starting from the state  $\vec{P} = \frac{1}{3}(1, 1, 1, 0, 0, 0, 0, 0, 0)$  generated by the first laser pulse, the MW and RF pulses generate the population vector  $\vec{P} = \frac{1}{3}(0, 0, 1, 0, 0, 1, 0, 0, 1)$ . Starting from this initial condition, the formal solution of Eq. (2) for the evolution of the populations during the second laser pulse is

$$\begin{aligned} \vec{P} = & \frac{1}{3} \left( 1 - e^{-k_S \tau_L} \frac{2k_I}{(3k_I - k_S)} - e^{-3k_I \tau_L} \frac{(k_I - k_S)}{(3k_I - k_S)}, \right. \\ & 1 - e^{-k_S \tau_L} \frac{2k_I}{(3k_I - k_S)} - e^{-3k_I \tau_L} \frac{(k_I - k_S)}{(3k_I - k_S)}, \\ & 1 - e^{-k_S \tau_L} \frac{2(k_I - k_S)}{(3k_I - k_S)} + e^{-3k_I \tau_L} \frac{2(k_I - k_S)}{(3k_I - k_S)}, \\ & \left. 0, 0, e^{-k_S \tau_L}, 0, 0, e^{-k_S \tau_L} \right). \end{aligned} \quad (3)$$

The general solution for arbitrary initial conditions is given in the appendix.

#### IV. EXPERIMENTAL RESULTS AND DISCUSSION

To test and optimize the preparation scheme outlined above, we performed experiments for different durations of the second laser pulse and analyzed the resulting state

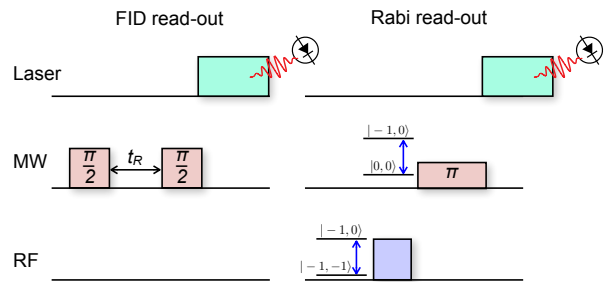


FIG. 2: Pulse sequences for measuring the free-induction decay of the electronic spin and the nuclear spin Rabi oscillation. For the FID scheme, the hard MW pulses are non-selective for all transitions from the  $m_S = 0$  to the  $m_S = -1$  state of the electron spin. In the Rabi scheme, the pulses are selective for the single transitions indicated in the figure.

by performing partial quantum state tomography. For this purpose, we measured Ramsey-type free induction decays, using the sequence shown in figure 2. The pulse sequence for this measurement consists of two identical  $\frac{\pi}{2}$  MW pulses separated by the free evolution time  $t_R$ . The first MW pulse generates a coherent superposition of the states  $m_S = 0$  and  $m_S = -1$  which subsequently evolves for a time  $t_R$ . The second MW pulse converts the coherence into population difference which is eventually measured by the read-out laser pulse. The detuning frequency  $\nu_{det}$ , determines the phase  $\phi$  of the second  $\frac{\pi}{2}$  MW pulse by  $\phi = \phi_c + 2\pi\nu_{det}t_R$  where the constant  $\phi_c$  is offset from the actual electronic transition frequency. A Fourier transform of the time-domain data generates the frequency-domain spectra. During these measurements we applied hard  $\frac{\pi}{2}$  MW pulses to excite all the three electron spin transitions corresponding to nuclear spin states  $m_I = 0, \pm 1$  between electronic spin states  $m_S = 0$  and  $-1$ .

Figure 3 shows four of the resulting spectra measured after the second laser pulse for pulse durations  $\tau_L = 5\text{ns}, 200\text{ns}, 480\text{ns}$  and  $4000\text{ns}$ . The arrows in the figure indicate the nuclear spin states to which the resonance lines are associated. Their amplitudes  $A_k$  are proportional to the population differences between the  $m_S = 0$  ground state of the electron spin and the  $m_S = -1$  state:  $A_k = P_{0,k} - P_{-1,k}$ , where  $k = 0, \pm 1$  indicates the nuclear spin quantum number.

Fig. 4 shows the measured amplitudes as a function of the laser pulse duration. For short laser pulses, all population differences vanish. For long durations, the populations of the three ground states  $|0, 0\rangle$  and  $|0, \pm 1\rangle$  converge to  $1/3$ , while the  $m_S = -1$  population vanishes, resulting in population differences of  $1/3$ . The experimental data are well consistent with the theoretical curves plotted using Eq. (3).

To determine the ground state populations, instead of population differences, we performed an additional experiment; we measured nuclear spin Rabi oscillations.

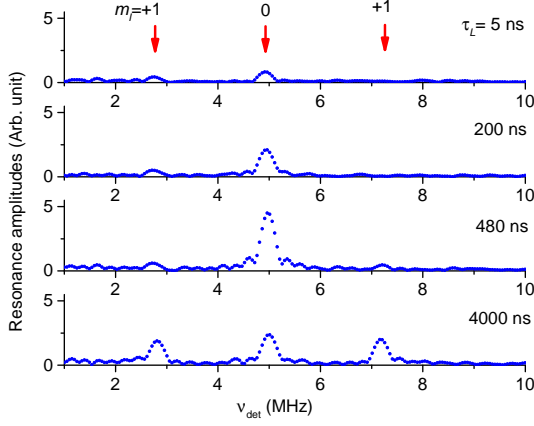


FIG. 3: ESR spectra, measured as Fourier transforms of Ramsey fringes for four different values of the laser pulse duration  $\tau_L$ . The amplitudes are proportional to the population difference between the  $m_S = 0$  and  $m_S = -1$  state for the three different nuclear spin states. The initial condition before applying the laser pulse with duration  $\tau_L$  was  $\vec{P} = \frac{1}{3}|_{\frac{3}{2}}(0, 0, 1, 0, 0, 1, 0, 0, 1)$ . The Ramsey measurements were done for free evolution times of up to 4  $\mu\text{s}$ , which limits the widths of the resonance lines in the spectra.

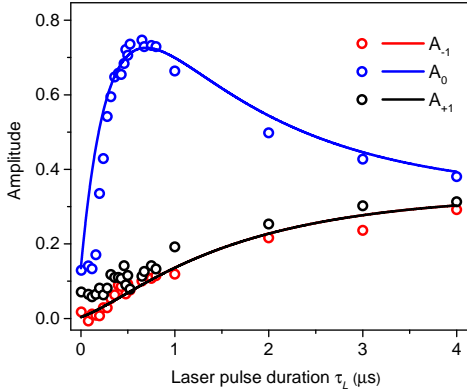


FIG. 4: Measured amplitudes of the resonance lines for the nuclear spin states  $|-1\rangle$ ,  $|+1\rangle$ , and  $|0\rangle$  and their sum  $A + A_{+1} + A_0$  (as mentioned in the graph legend) along with the corresponding theoretical curves as described in Eq. 3.

Fig. 2 (rhs) shows the pulse sequence used for the Rabi measurements. It consists of two consecutive pulses; one RF Rabi pulse with variable duration  $t_{RF}$  and one MW  $\pi$  pulse. The RF pulse exchanges the populations of the  $|-1, 0\rangle$  and the  $|-1, -1\rangle$  states and the MW pulse those of the  $|-1, 0\rangle$  and  $|0, 0\rangle$  states. Taking into account that  $P_{-1, -1}$  vanishes before this measurement, the readout pulse detects the total population of the electronic  $|0\rangle$

state as

$$P_{m_S=0}(t_{RF}) = P_{0,-1} + P_{0,+1} + P_{-1,0} \frac{1 + \cos \omega_1 t_{RF}}{2},$$

where  $\omega_1$  is the Rabi frequency of the RF field and the populations  $P_{i,j}$  refer to the state before the pulse sequence. The oscillation amplitude of the Rabi oscillation is thus proportional to the population  $P_{-1,0}$ . Fig. 5 (a) shows a typical Rabi oscillation for a short laser pulse ( $\tau_L = 5$  ns) and Fig. 5 (b) shows the observed values of  $P_{-1,0}$  as a function of  $\tau_L$ .

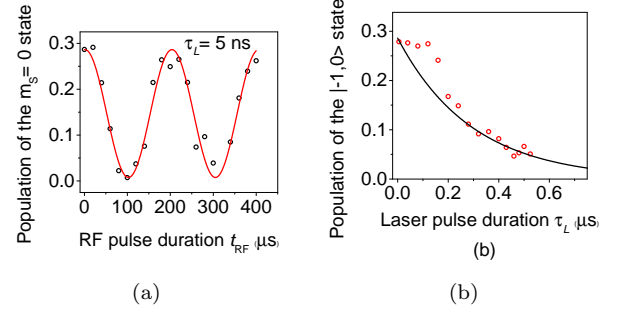


FIG. 5: (a) Rabi oscillation data between the  $|-1, -1\rangle$  and  $|-1, 0\rangle$  states for  $\tau_L = 5$  ns. (b) Experimentally measured values of  $P_{-1,0}$  (circles) as a function of  $\tau_L$  with the theoretical curve given by Eq. (3) with  $k_S = 1/0.217 \mu\text{s}$ .

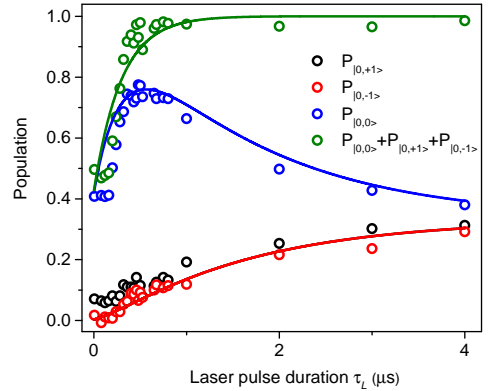


FIG. 6: Measured populations of the three ground states  $|0, -1\rangle$ ,  $|0, +1\rangle$ ,  $|0, 0\rangle$  and their sum as a function of the laser pulse duration  $\tau_L$ , together with the fitted curves.

Once  $P_{-1,0}$  is determined, it is straightforward to calculate  $P_{0,0}$  using the simple relationship  $A_0(\tau_L) + P_{-1,0}(\tau_L) = P_{0,0}(\tau_L)$ . Fig. 6 shows all three populations  $P_{0,0}$ ,  $P_{0,-1}$  and  $P_{0,+1}$  for the initial condition  $\vec{P} = \frac{1}{3}|_{\frac{3}{2}}(0, 0, 1, 0, 0, 1, 0, 0, 1)$  as a function of the laser

pulse duration  $\tau_L$ . The experimental data were normalized by considering that the sum of all nine populations must add up to 1. The population of the  $|0, 0\rangle$  state increases rapidly, with a rate  $k_S$ , until it goes through a maximum. On a longer time scale determined by  $k_I$ , all three populations tend towards the equilibrium value of  $1/3$ . The experimental data for the individual nuclear spin sub-states, as well as the total population of the  $m_S = 0$  state were fitted with the theoretical expressions of Eq. (3). The resulting values of the time constants were  $1/k_S = 0.29 \pm 0.02 \mu s$  and  $1/k_I = 4.7 \pm 0.4 \mu s$ . The fact that the effect of the laser pulse illumination started with a constant time delay in the experimental data, has been taken care of by adding a constant value  $\tau_d$  with  $\tau_L$  in the rate equation model. We estimated  $\tau_d = 45 ns$ . The maximum population (77.8 %) of the  $|0, 0\rangle$  state is obtained for a pulse duration  $\tau_L \approx 0.48 \mu s$ . For the  $m_I = \pm 1$  states, the amplitudes  $A_{-1}$  and  $A_{+1}$ , represent directly the populations  $P_{0,-1}$  and  $P_{0,+1}$ , as the population of the  $|-1, -1\rangle$  and  $|-1, +1\rangle$  states vanish.

Different mechanisms lead to loss of nuclear spin polarization during laser excitation [33, 34]. For instance, under laser illumination, hyperfine-induced electron-nuclear spin flip-flop processes have a dominant effect on the nuclear spin lifetime  $T_1$  when the applied magnetic field is such that the system is close to the excited-state level anticrossing point (LAC). In addition, coupling of the electronic and nuclear spin with phonons can lead to depolarization of the nuclear spin. In our case, since we performed experiments at the field of 6.1 mT which is well below the LAC ( $\approx \pm 50$  mT) and spin-orbit coupling has negligible effect in the  $m_S = 0$  state, the above mentioned reasons have negligible influence on  $T_1$ . In case of spin flip-flop process,  $k_I$  includes only the transitions with selection rule  $\Delta m_I = \pm 1$ . Comparing the experimental data with both models, we found that the data fits better to the model where flips with  $\Delta m_I = \pm 1$  and  $\pm 2$  occur. We assume that a dominant contribution to nuclear depolarization is the different energy eigenstates in the ground and excited state: The optical excitation thus projects the nuclear spin eigenstates of the electronic ground state onto a superposition of nuclear spin states in the electronically excited state. Another contribution is the conversion of the  $NV^-$  centers to  $NV^0$  with increasing laser pulse duration [39]. The two charge states of the NV center have different hyperfine coupling and different nuclear quadrupole interactions. This changes the energy splitting between the nuclear sublevels and the nuclear spin eigenstates. Accordingly, a change of charge state may be accompanied by a loss of spin polarization. In addition, the measured value of  $T_1$  in the  $NV^0$  state is significantly shorter than in the  $NV^-$  state [40–42]. The parameter  $k_I$  summarizes this overall depolarization rate of the nuclear spin for the given laser irradiation.

To further improve the purity of the  $|0, 0\rangle$  state in the  $m_S = 0$  subspace, we used two selective microwave  $\pi$  pulses MW3 and MW4, both with the same pulse duration of  $3.874 \mu s$ , to transfer the population from the

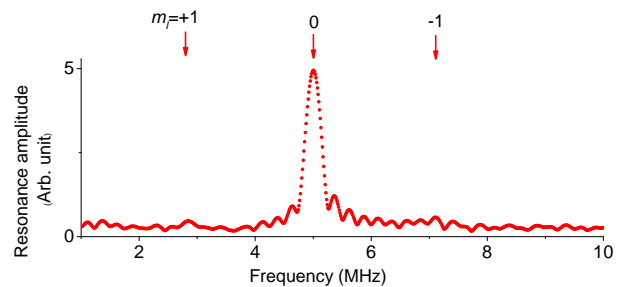


FIG. 7: Experimental spectrum showing the amplitudes  $A_0$  and  $A_{\pm 1}$  measured using the read-out procedure shown in Fig. 2, after applying the microwave pulses MW3 and MW4 shown in Fig. 1.

$|0, -1\rangle$  to the  $|+1, -1\rangle$  state and from the  $|0, +1\rangle$  to the  $|+1, +1\rangle$  state, respectively. The resulting spin configuration was read out by performing free-induction-decay measurements of the electronic spin. The pulse sequence containing the MW3 and MW4 pulses is shown in the 2<sup>nd</sup> part of Fig. 1 and the FID read out pulses are shown in Fig. 2. Fig. 7 shows the resulting spectrum, which contains a single distinct peak indicating the population of the  $|0, 0\rangle$  state. The measured amplitudes show that  $> 96\%$  of the population of the  $m_S = 0$  subspace is in the  $|0, 0\rangle$  state.

Apart from the optically induced nuclear spin relaxation, the attainable polarization is also limited by experimental imperfections. In order to study the effect of imperfection of the pulse length on the attainable purity of the  $|0, 0\rangle$  state, we have calculated the derivative of  $P_{0,0}$  with respect to each pulse angle while keeping the other three angles fixed at  $\pi$ . We obtained  $\Delta P_{0,0} = \frac{(\Delta \theta_i)^2}{4}$ . The uncertainty in the pulse angles of the MW and RF pulses is 1.5% and 3.2% which leads to respectively 0.56% and 2.56% loss in the final purity of the  $|0, 0\rangle$  state. In addition, an imperfect initial state influences the achievable purity. If the first laser pulse initializes the system to a state  $\vec{P} = [P_1, P_2, 1 - (P_1 + P_2), 0, 0, 0, 0, 0, 0]$ , the final polarization  $P_{0,0}$  becomes  $P_{0,0} = 0.7858 - 0.029(P_1 + P_2)$  with the boundary conditions  $0 \leq P_1 \leq 1$ ,  $0 \leq P_2 \leq 1$  and  $P_1 + P_2 \leq 1$ . The relation indicates that the purity of  $|0, 0\rangle$  state is maximum when  $P_1 = P_2 = 0$  whereas the purity decreases as  $P_1$  and  $P_2$  increase. The average absolute deviation from the mean value of the experimentally measured quantities  $P_1$  and  $P_2$  are 1.65% and 1.32% respectively, which corresponds to 0.086% loss in the achievable purity of the  $|0, 0\rangle$  state.

## V. CONCLUSION

To summarize, we have employed a procedure for the purification of the quantum state of a two-qubit system associated with a single NV center in diamond. Laser pulses can initialize the electronic spin. To initialize also

the nuclear spin, we first initialized the electron spin, swapped the states of the electronic and the nuclear spin and then again initialized the electronic spin, which is quite similar to the sequence used by Pagliero et al. [20]. However, the present work provides a detailed understanding of the population transfer between the relevant states under optical illumination and a qualitative estimation of the occupation probabilities of different individual quantum states. The corresponding values were obtained by performing partial quantum state tomography. We were able to establish an effective rate equation model which is in excellent agreement with the experimental results. The interpretation of the results using the formulated theory enabled us to determine the relevant rate constants and the optimal duration of the laser pulse. Thus, the optimal sequence allows one to prepare an arbitrary state of the system with high purity, which is essential for coherently controlled experiments on NV centers in diamond. Although the resultant purity is limited by the initial laser-induced electronic polarization of  $m_S = 0$  state and nuclear depolarization, the procedure offers the benefit that it can be implemented with flexible magnetic field values. Finally, we have improved the purity of the  $|0, 0\rangle$  state in

the  $m_S = 0$  subspace. Enhancing the occupation probability of the target input state in a certain computational space can result in a better performance in experiments like quantum gate operations. For instance, in an experiment where dynamical decoupling was applied to implement protected operation of a controlled rotation gate in a definite subspace [15], an enhanced purity of the input state increases the signal-to-noise ratio.

### Acknowledgments

We gratefully acknowledge useful discussions with K. Rama Koteswara Rao, Manpreet Kaler and Fabian Lehmann. We also sincerely thank Nabeel Aslam and Matthias Pfender for useful discussions. This work was supported by the DFG through grants 192/19-2, 192/34-1 and by the MERCUR foundation through grant Pr-2013-0003. We acknowledge financial support by Deutsche Forschungsgemeinschaft and TU Dortmund Technical University within the funding programme Open Access Publishing.

- 
- [1] I. Aharonovich, *Adv. Opt. Mater.* **2**, 911 (2014).  
 [2] F. Jelezko, T. Gaebel, I. Popa, M. Domhan, A. Gruber, and J. Wrachtrup, *Phys. Rev. Lett.* **93**, 130501 (2004).  
 [3] M. V. G. Dutt, L. Childress, L. Jiang, E. Togan, J. Maze, F. Jelezko, A. S. Zibrov, P. R. Hemmer, and M. D. Lukin, *Phys. Rev. Lett.* **316**, 1312 (2007).  
 [4] P. Neumann, N. Mizuochi, F. Rempp, P. Hemmer, H. Watanabe, S. Yamasaki, V. Jacques, T. Gaebel, F. Jelezko, and J. Wrachtrup, *Science* **320**, 1326 (2008).  
 [5] G. Balasubramanian, P. Neumann, D. Twitchen, M. Markham, R. Kolesov, N. Mizuochi, J. Isoya, J. Achard, J. Beck, and J. T. et al., *Nat. Mater.* **8**, 383 (2009).  
 [6] Y. Chu, M. Markham, D. J. Twitchen, and M. D. Lukin, *Phys. Rev. A* **91**, 021801 (2015).  
 [7] C. G. Y. et al., *PNAS* **110**, 7595 (2013).  
 [8] F. Jelezko and J. Wrachtrup, *Phys. Stat. Sol. (a)* **13**, 3207 (2006).  
 [9] H. B. et al., *Phys. Rev. Lett.* **108**, 043604 (2012).  
 [10] A. S. et al., *Phys. Rev. Lett.* **108**, 143601 (2012).  
 [11] S. D. Barrett and P. Kok, *Phys. Rev. A* **71**, 060310 (2005).  
 [12] A. M. Stoneham, A. H. Harker, and G. W. Morley, *J. Phys.: Condens. Matter* **21**, 364222 (2009).  
 [13] J. H. Shim, I. Niemeyer, J. Zhang, and D. Suter, *Phys. Rev. A* **87**, 012301 (2013).  
 [14] L. R. et al., *Nature* **477**, 574 (2011).  
 [15] J. Zhang and D. Suter, *Phys. Rev. Lett.* **115**, 110502 (2015).  
 [16] P. C. M. et al., *Science* **336**, 1283 (2012).  
 [17] T. Gaebel, M. Domhan, I. Popa, C. Wittmann, P. Neumann, F. Jelezko, J. R. Rabeau, N. Stavrias, A. D. Greentree, S. Prawer, et al., *Nature Phys.* **2**, 408 (2006).  
 [18] L. C. et al., *Science* **314**, 281 (2006).  
 [19] P. Jamonneau, G. Hétet, A. Dréau, J.-F. Roch, and V. Jacques, *Phys. Rev. Lett.* **116**, 043603 (2016).  
 [20] D. Pagliero, A. Laraoui, J. D. Henshaw, and C. A. Meriles, *Applied Physics Letters* **105**, 242402 (2014).  
 [21] B. E. Kane, *nature* **393**, 133 (1998).  
 [22] N. A. Gershenfeld and I. L. Chuang, *science* **275**, 350 (1997).  
 [23] A. W. Overhauser, *Physical Review* **92**, 411 (1953).  
 [24] A. Abragam and M. Goldman, *Reports on Progress in Physics* **41**, 395 (1978).  
 [25] S. Sukhenko and K. Salikhov, *Chemical physics* **98**, 431 (1985).  
 [26] K. Tateishi, M. Negoro, S. Nishida, A. Kagawa, Y. Morita, and M. Kitagawa, *Proceedings of the National Academy of Sciences* **111**, 7527 (2014).  
 [27] J. P. King, K. Jeong, C. C. Vassiliou, C. S. Shin, R. H. Page, C. E. Avalos, H.-J. Wang, and A. Pines, *Nature Communications* **6** (2015).  
 [28] J. Scheuer, I. Schwartz, Q. Chen, D. Schulze-Sinninghausen, P. Carl, P. Höfer, A. Retzker, H. Sumiya, J. Isoya, B. Luy, et al., *New Journal of Physics* **18**, 013040 (2016).  
 [29] G. A. Álvarez, C. O. Bretschneider, R. Fischer, P. London, H. Kanda, S. Onoda, J. Isoya, D. Gershoni, and L. Frydman, *Nature communications* **6** (2015).  
 [30] A. L. Falk, P. V. Klimov, V. Ivády, K. Szász, D. J. Christle, W. F. Koehl, Á. Gali, and D. D. Awschalom, *Physical review letters* **114**, 247603 (2015).  
 [31] A. Dréau, P. Spinicelli, J. Maze, J.-F. Roch, and V. Jacques, *Physical review letters* **110**, 060502 (2013).  
 [32] J. J. Pla, K. Y. Tan, J. P. Dehollain, W. H. Lim, J. J. Morton, F. A. Zwanenburg, D. N. Jamieson, A. S. Dzu-

- rak, and A. Morello, *Nature* **496**, 334 (2013).
- [33] P. Neumann, J. Beck, M. Steiner, F. Rempp, H. Fedder, P. R. Hemmer, J. Wrachtrup, and F. Jelezko, *Science* **329**, 542 (2010).
- [34] P. London, J. Scheuer, J.-M. Cai, I. Schwarz, A. Retzker, M. B. Plenio, M. Katagiri, T. Teraji, S. Koizumi, J. Isoya, et al., *Phys. Rev. Lett.* **111**, 067601 (2013).
- [35] L. Robledo, H. Bernien, T. van der Sar, and R. Hanson, *New Journal of Physics* **13**, 025013 (2011).
- [36] D. P. DiVincenzo, *Fortschr. Phys.* **48**, 7583 (2000).
- [37] V. Jacques, P. Neumann, J. Beck, M. Markham, D. Twitchen, J. Meijer, F. Kaiser, G. Balasubramanian, F. Jelezko, and J. Wrachtrup, *Phys. Rev. Lett.* **102**, 057403 (2009).
- [38] M. Steiner, P. Neumann, J. Beck, F. Jelezko, and J. Wrachtrup, *Phys. Rev. B* **81**, 035205 (2010).
- [39] N. Aslam, G. Waldherr, P. Neumann, F. Jelezko, and J. Wrachtrup, *New Journal of Physics* **15**, 013064 (2013).
- [40] G. Waldherr, J. Beck, M. Steiner, P. Neumann, A. Gali, T. Frauenheim, F. Jelezko, and J. Wrachtrup, *Phys. Rev. Lett.* **106**, 157601 (2011).
- [41] X.-D. Chen, L.-M. Zhou, C.-L. Zou, C.-C. Li, Y. Dong, F.-W. Sun, and G.-C. Guo, *Physical Review B* **92**, 104301 (2015).
- [42] M. Loretz, H. Takahashi, T. Segawa, J. Boss, and C. Degen, arXiv preprint arXiv:1612.08104 (2016).

## VI. APPENDIX

The matrix  $M(k_S, k_I)$  describing the effect of the laser pumping on the electronic and nuclear spin is,  $M(k_S, k_I) =$

$$\begin{bmatrix} -2k_I & k_I & k_I & k_S & 0 & 0 & k_S & 0 & 0 \\ k_I & -2k_I & k_I & 0 & k_S & 0 & 0 & k_S & 0 \\ k_I & k_I & -2k_I & 0 & 0 & k_S & 0 & 0 & k_S \\ 0 & 0 & 0 & -k_S & 0 & 0 & 0 & 0 & 0 \\ 0 & 0 & 0 & 0 & -k_S & 0 & 0 & 0 & 0 \\ 0 & 0 & 0 & 0 & 0 & -k_S & 0 & 0 & 0 \\ 0 & 0 & 0 & 0 & 0 & 0 & -k_S & 0 & 0 \\ 0 & 0 & 0 & 0 & 0 & 0 & 0 & -k_S & 0 \\ 0 & 0 & 0 & 0 & 0 & 0 & 0 & 0 & -k_S \end{bmatrix}$$

where the population vector is depicted with the order  $(m_S, m_I) = (0, -1; 0, +1; 0, 0; -1, -1; -1, +1; -1, 0; +1, -1; +1, +1; +1, 0)$ .

For an initial state  $\vec{P} = (P_1, P_2, P_3, P_4, P_5, P_6, P_7, P_8, P_9)$  and after the second laser pulse of duration  $\tau_L$ , the resulting population vector is

$$\begin{aligned} \vec{P} = & \frac{1}{3} \left( 1 + \frac{ae^{-3k_I\tau_L} + 3be^{-3k_S\tau_L}}{(3k_I - k_S)}, 1 + \frac{3ce^{-k_S\tau_L} + fe^{-3k_I\tau_L}}{(3k_I - k_S)}, \right. \\ & 1 + \frac{3ge^{-k_S\tau_L} + he^{-3k_I\tau_L}}{(3k_I - k_S)}, 3P_4e^{-k_S\tau_L}, 3P_5e^{-k_S\tau_L}, \\ & 3P_6e^{-k_S\tau_L}, \\ & \left. 3P_7e^{-k_S\tau_L}, 3P_8e^{-k_S\tau_L}, 3P_9e^{-k_S\tau_L} \right), \end{aligned}$$

where

$$a = k_S - 3k_I P_3 + 6k_I P_1 - 3k_I P_2 - 3k_S P_1 - 3k_S P_4 - 3k_S P_7,$$

$$b = k_I P_3 - k_I + k_I P_1 + k_I P_2 + k_S P_4 + k_S P_7,$$

$$c = k_I P_3 - k_I + k_I P_1 + k_I P_2 + k_S P_5 + k_S P_8,$$

$$f = k_S - 3k_I P_3 - 3k_I P_1 + 6k_I P_2 - 3k_S P_5 - 3k_S P_2 - 3k_S P_8,$$

$$g = k_S - k_I - k_S(P_5 + P_4 + P_7 + P_8) + (k_I - k_S)(P_3 + P_1 + P_2)$$

and

$$h = 6k_I P_3 - 2k_S + 3k_S(P_5 + P_4 + P_7 + P_8) - 3(k_I - k_S)(P_1 + P_2).$$